Inverse design of third-order Dirac exceptional points in photonic crystals

Zin Lin[1],[*] Adi Pick[2],[3] Marko Lončar[1], and Alejandro W. Rodriguez[4]

[1]*John A. Paulson School of Engineering and Applied Sciences, Harvard University, Cambridge, MA 02138*
[2]*Department of Physics, Harvard University, Cambridge, MA 02138*
[3]*Department of Mathematics, Massachusetts Institute of Technology, Cambridge, MA 02139 and*
[4]*Department of Electrical Engineering, Princeton University, Princeton, NJ, 08544*
(Dated: May 23, 2016)

We propose a novel inverse-design method that enables brute-force discovery of photonic crystal (PhC) structures with complex spectral degeneracies. As a proof of principle, we demonstrate PhCs exhibiting third-order Dirac points formed by the *accidental* degeneracy of modes of monopolar, dipolar, and quadrupolar nature. We show that under suitable conditions, these modes can coalesce and form a third-order exceptional point (EP3), leading to diverging Petermann factors. We show that the spontaneous emission (SE) rate of emitters at such EP3s, related to the local density of states, can be enhanced by a factor of 8 in purely lossy (passive) structures, with larger enhancements $\sim \sqrt{n^3}$ possible at exceptional points of higher order n or in materials with gain.

PACS numbers: Valid PACS appear here

Dirac cones in photonic systems have received much attention because of their connections to intriguing optical properties, enabling large-area photonic-crystal (PhC) surface-emitting lasers [1], zitterbewegung of photons [2], appearance of zero-index behavior [3, 4], and as precursors to nontrivial topological effects [5–7]. Recent work also showed that Dirac-point degeneracies can give rise to rings of exceptional points [8]. An exceptional point (EP) is a singularity in a non-Hermitian system where two or more eigenvectors and their corresponding complex eigenvalues coalesce, leading to a non-diagonalizable, defective Hamiltonian [9, 10]. EPs have been studied in various physical contexts, most notably lasers and atomic as well as molecular systems [11, 12]. In recent decades, interest in EPs has been re-ignited in connection with non-Hermitian parity-time symmetric systems [13], especially optical media involving carefully designed gain and loss profiles [14–20], where they can lead to intriguing phenomena such as enhanced spontaneous emission (SE) [21, 22], chiral modes [23], directional transport [24, 25] and anomalous lasing behavior [26–28]. Also recently, it became possible to directly observe EPs in photonic crystals (PhC) [8] and optoelectronic microcavities [29]. Thus far, however, only second-order EPs (EP2) (where only two modes coalesce) have been proposed in the context of photonic radiators: in fact, apart from a few mathematical analyses [30–32] or very recently, acoustic systems [33], there has been little or no investigation into appearance of EPs of higher order (where more than two modes collapse) in complex photonic geometries.

In this letter, we propose a powerful inverse-design method based on topology optimization that allows automatic discovery of complex photonic structures supporting Dirac points (DP) formed out of the *accidental* degeneracy [34] of modes belonging to different symmetry representations. In particular, we show that such higher-order DPs can be exploited to create third-order exceptional points (EP3) along with complex contours of EP2. In addition, we exploit coupled-mode theory to derive conditions under which such EP3s can exist and extend recent work [22] to consider the possible enhance-

ments and spectral modifications in the SE rate of emitters. Specifically, we show that the local density of states at a EP3 can be enhanced 8-fold (in passive systems) and can exhibit a cubic Lorentzian spectrum under special conditions. More generally, we find that the enhancement factor $\sim \sqrt{n^3}$ with increasing EP order n, whilst even larger enhancements are expected under gain [22]. Our findings provide the foundations for future discoveries of complex structures with unusual or exotic modal properties currently out of the reach of conventional, intuitive design principles.

Dirac cones and Dirac EPs are typically designed by exploiting degeneracies between modes of different symmetry representations, often in simple geometries involving cylindrical pillars or holes on a square or triangular lattice [3, 35]. These singularities are typically of order two (comprising two interacting modes) and arise partly out of some underlying lattice symmetry (e.g. C_{4v} or C_{3v}) and through the fine-tuning of a few geometric parameters [3, 36]. For instance, in Ref. 8, it was recently demonstrated that a Dirac point (DP) at the Γ point of a PhC with C_{4v} symmetry can give rise to a ring of EP2s. Such a DP is formed by a degeneracy involving modes of both monopolar (M) and dipolar (D) nature, which transform according to A and E representations of the C_{4v} group [3, 36]. Even though the degeneracy consists of one monopole and two dipoles, the induced EP is of the second order, with only the monopole and one of the dipoles colliding, while the coalescence of the dipole partner is prevented by their symmetry [8]. Below, we show that an EP3 can be induced by a completely "accidental" third-order degeneracy (D3) at Γ, involving modes of monopolar (M), dipolar (D) and quadrupolar (Q) nature arising in a novel, inverse-designed PhC structure lacking C_{4v} symmetry.

Coupled-mode analysis.— The band structure in the vicinity of such a D3 can be modeled by an approximate Hamiltonian of the form [35]:

$$\mathcal{H} = \begin{pmatrix} \omega_0 & v_{\mathrm{MD}}k_x & 0 \\ v_{\mathrm{MD}}k_x & \omega_0 & v_{\mathrm{QD}}k_y \\ 0 & v_{\mathrm{QD}}k_y & \omega_0 \end{pmatrix} \qquad (1)$$

Here, v_{ij}, $i, j \in \{M, D, Q\}$ characterizes the mode mixing away from the Γ point, to first order in $\mathbf{k}$ [35]. Note that the diagonalization of this Hamiltonian yields a completely real band structure comprising a Dirac cone and a flat band,

$$\omega = \omega_0, \ \omega_0 \pm \sqrt{v_{MD}^2 k_x^2 + v_{QD}^2 k_y^2} \tag{2}$$

To induce an EP, non-Hermiticity can be introduced by the addition of a small imaginary perturbation to the Hamiltonian,

$$\mathcal{H} = \begin{pmatrix} \omega_0 + i\gamma_M & v_{MD}k_x & 0 \\ v_{MD}k_x & \omega_0 + i\gamma_D & v_{QD}k_y \\ 0 & v_{QD}k_y & \omega_0 + i\gamma_Q \end{pmatrix} \tag{3}$$

with $\gamma > 0$ (< 0) representing a small amount of absorption (amplification) or radiation. A EP3 is obtained by demanding that the characteristic polynomial of (3) have vanishing derivatives up to second order,

$$\det(\mathcal{H} - \omega\mathbb{I}) = P(\omega) = 0, \tag{4}$$
$$P'(\omega) = 0, \tag{5}$$
$$P''(\omega) = 0. \tag{6}$$

Solving the above equations for ω, k_x, and k_y yields the EP3:

$$\omega^{EP3} = \omega_0 + \frac{i}{3}(\gamma_M + \gamma_D + \gamma_Q) \tag{7}$$

$$k_x^{EP3} = \pm\frac{1}{3v_{MD}}\sqrt{\frac{(\gamma_D + \gamma_Q - 2\gamma_M)^3}{3(\gamma_Q - \gamma_M)}} \tag{8}$$

$$k_y^{EP3} = \pm\frac{1}{3v_{QD}}\sqrt{\frac{(2\gamma_Q - \gamma_M - \gamma_D)^3}{3(\gamma_Q - \gamma_M)}} \tag{9}$$

where, any choice of distinct γ leading to real $\mathbf{k}$ induces an EP3. In a lattice with C_{4v} symmetry, this condition cannot be satisfied, unless the symmetry relating the two dipolar modes is severely and intentionally broken. Such a design would necessitate an overlay of spatially varying regions of gain/loss, a scenario that seems experimentally challenging. In contrast, we now present a novel design method that can discover PhC geometries supporting "accidental" and tunable D3s.

Inverse-design method.— We construct an accidental D3 by employing a large-scale optimization strategy for automatically discovering novel topologies and geometries impossible to conceive from conventional intuition alone. One such strategy, known as topology optimization (TO), employs powerful gradient-based numerical algorithms capable of handling a very large design space, typically considering every pixel or voxel as a degree of freedom (DOF) in an extensive 2d or 3d computational domain. Such techniques have been gaining traction and were recently applied to problems involving linear input/output coupling of light [37–39], cavity Purcell enhancement [40], and nonlinear frequency conversion [41]. In this work, we apply TO to the problem of inverse-designing the band structure of a PhC to support spectral DP degeneracies and EP singularities.
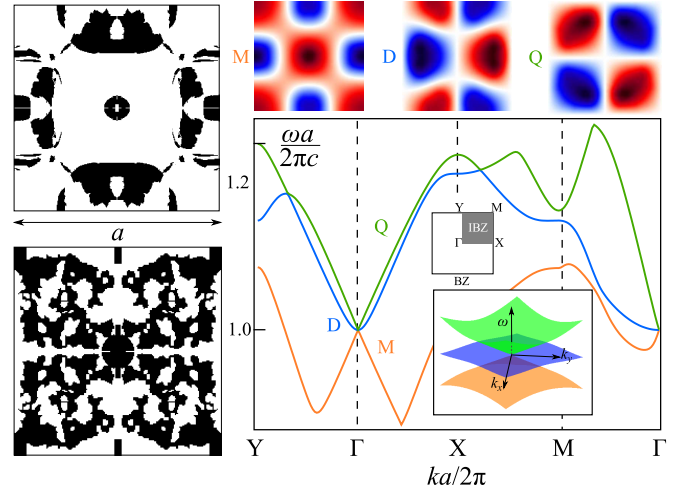

FIG. 1. Inverse-designed 2d square lattices comprising either low-index ($n = 2$, upper left) or high-index ($n = 3$, lower left) materials in air (white regions), with periodicity $a/\lambda = 1.05$ and $a = 0.6/\lambda$, respectively. Note that both unit cells lack C_{4v} symmetry, but retain C_{2v} symmetry by design. Lower right: band structure of the low-index (upper) lattice, revealing a Dirac point induced by the presence of an *accidental* third-order degeneracy (D3) of monopolar (M), dipolar (D), and quadrupolar (Q) modes (upper insets), leading to linear Dirac dispersion accompanied by a quadratic flat band at the Γ point. A schematic of the Brillouin zone (BZ) denoting high-symmetry $\mathbf{k}$ points (Y, Γ, X, M) is also shown. Due to the lack of C_{4v} symmetry, the dispersion along the X and Y directions differ.

Our approach extends the work of Ref. 40, which showed that it is possible to design a structure supporting a resonant mode at some arbitrary frequency by maximizing the time-averaged power output $f = -\text{Re}\left[\int \mathbf{J}^* \cdot \mathbf{E} \, d\mathbf{r}\right]$ emitted from a time harmonic current source $\mathbf{J}$ at the desired frequency ω, where the electric field response $\mathbf{E}$ is given by the solution of Maxwell's equations, $\nabla \times \frac{1}{\mu}\nabla \times \mathbf{E} - \omega^2\epsilon(\mathbf{r})\mathbf{E} = i\omega\mathbf{J}$ [40]. To ensure that the designed resonance has the requisite modal profile, the current $\mathbf{J}$ must be judiciously constructed. For example, to design a transverse magnetic (TM) polarized monopolar mode (M) at the Γ point of a PhC, $\mathbf{J}$ should can be chosen as a point dipole $\mathbf{J} = \delta(\mathbf{r}-\mathbf{r}_0)\mathbf{e}_z$ at the center $\mathbf{r}_0$ of the unit cell. Once the objective function f is identified, its gradient with respective to $\epsilon(\mathbf{r})$ can be calculated by the so-called adjoint variable method [37, 40] (see the supplement for details) and then supplied to any large-scale gradient-based optimization algorithm such as the method of moving asymptotes (MMA) [42]. To design structures supporting multiple modes at the same frequency with the requisite (M, D, Q) symmetries, we seek a maxmin formulation in which one maximizes the minimum of $\{f_M, f_D, f_Q\}$, with currents chosen to ensure fields with the desired symmetries, discussed in detail in the supplementary materials [SM].

Our topology optimization framework can be exploited to design high-order degeneracies with distinct modal properties in arbitrary material systems and photonic structures. Here, we use it to demonstrate the appearance of third-order degen-
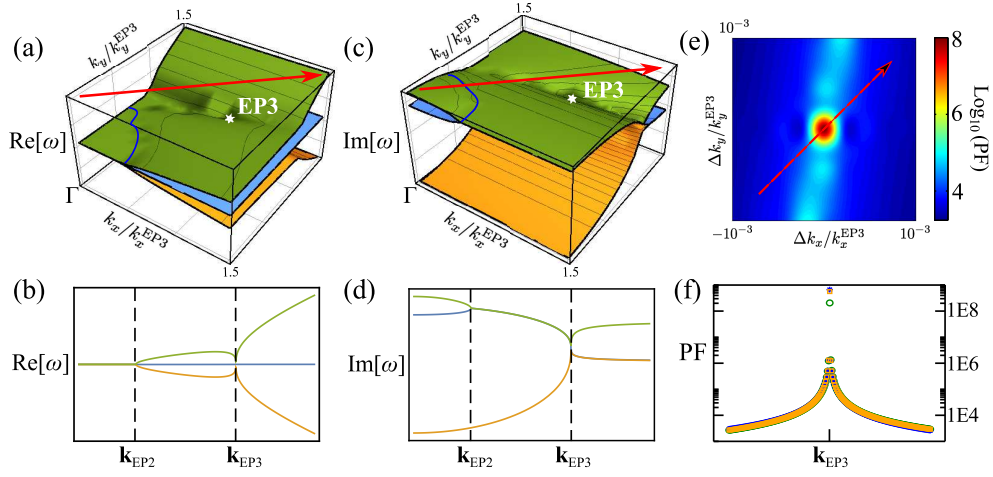
FIG. 2. (a) Real and (c) imaginary eigenfrequencies as a function of k_x and k_y in the vicinity of a third order exceptional point (EP3) of the structure described in Fig. 1, located at $\mathbf{k}^{\mathrm{EP3}} \approx \{7, 1.8\} \times 10^{-5} \left(\frac{2\pi}{a}\right)$ (red dot). The blue contours denote regions of second-order exceptional points where two of the three modes coalesce. The plots in (b) and (d) show the corresponding band structures along the $\mathbf{k}$ lines marked by red arrows. (e) Contour plot showing the enhanced Petermann factor (PF) associated with one of the modes in the vicinity of the EP3, and (e) corresponding enhancement along the direction shown by the red arrow, for all three modes.

eracies in binary dielectric/air square lattices. Figure 1(left) shows two such structures, involving materials of either low ($n = 2$, upper) or high ($n = 3$, lower) refractive indices (in air) and periodicities $a = 1.05\,\lambda$ and $a = 0.6\,\lambda$, respectively, where λ is the design wavelength in vacuum. Note that such refractive indices are typical for common materials such as silicon nitride, lithium niobate, diamond, silicon, alumina, or many low and high-index ceramics at optical, microwave, and terahertz frequencies. We focus our discussion on the low-index structure, leaving details of the high-index design to the [SM]. Noticeably, the band structure of the low-index lattice exhibits a D3 comprising M, D and Q modes at the Γ point, shown in Fig. 1 (lower right). Note that since the optimized PhC lacks C_{4v} symmetry (but possesses C_{2v}), there is only one dipolar mode at the designated frequency and hence, the degeneracy of the three modes is completely *accidental*: potential mode mixing and avoided crossings at the Γ point are prevented by the corresponding mirror symmetries. In the vicinity of the tri-modal degeneracy, the band structure exhibits conical Dirac dispersion accompanied by a quadratic flat band. While general rules regarding the occurrence of Dirac point (DP) dispersion in the vicinity of a modal degeneracy are well understood from group theoretic considerations, e.g. as arising from *two* different irreducible representations [36], to our knowledge our TO-designed PhC is the first demonstration of a DP formed by *three* degenerate modes belonging to *three* different representations, namely the A_1, A_2 and B_1 representations of the C_{2v} group.

Third-order exceptional point.— The third order Dirac degeneracy of Fig. 1 can be straightforwardly linked to an EP3 through the introduction of non-Hermiticity, i.e. material loss, gain, or open boundaries (radiation). Here, we consider such an EP3 by introducing a small imaginary part in the dielectric constant, $\kappa = \sqrt{\mathrm{Im}[\epsilon]} = 0.005$, representing intrinsic material loss and resulting in small decay rates $\{\gamma_{\mathrm{M}}, \gamma_{\mathrm{D}}, \gamma_{\mathrm{Q}}\}/\omega_0 \approx \{3.6, 4.3, 4.2\} \times 10^{-4}$. From (8), (9), it follows that there exists an EP3 at $\mathrm{Re}[\omega_{\mathrm{EP3}}] \approx \omega_0$, $\mathrm{Im}[\omega_{\mathrm{EP3}}] \approx 4 \times 10^{-4}(\frac{2\pi c}{a})$, $k_x^{\mathrm{EP3}} \approx 7 \times 10^{-5} \left(\frac{2\pi}{a}\right)$ and $k_y^{\mathrm{EP3}} \approx 1.8 \times 10^{-5} \left(\frac{2\pi}{a}\right)$ [SM]. Figure 2(a) and (c) show the band structure in the vicinity of the Γ point, along with slices, Fig. 2(b) and (d), indicated by blue arrows, illustrating the coalescence of both the real and imaginary mode frequencies. Yet another interesting feature of the dispersion landscape is that, apart from the EP3, there also exists a contour of EP2 (blue lines), defined by $P(\omega; k_x, k_y) = 0$, $P'(\omega; k_x, k_y) = 0$, similar to the ring of EP2 observed in Ref. 8.

A defining signature of non-Hermitian systems is that eigenvectors are no longer orthogonal. Rather, they are biorthogonal [10] in the sense of an unconjugated "inner product" between left and right eigenvectors, $\left(\Psi_n^{\mathrm{L}}\right)^{\mathrm{T}} \Psi_m^{\mathrm{R}} = \delta_{nm}$, defined such that $A\Psi^{\mathrm{R}} = \omega^2 \Psi^{\mathrm{R}}$ and $A^{\mathrm{T}}\Psi^{\mathrm{L}} = \omega^2 \Psi^{\mathrm{L}}$, where A is the Maxwell operator $\hat{\epsilon}^{-1}(\nabla + i\mathbf{k}) \times \frac{1}{\mu}(\nabla + i\mathbf{k}) \times$ under Bloch boundary conditions at a specific $\mathbf{k}$, $\hat{\epsilon}$ is the diagonal permittivity tensor $\epsilon(\mathbf{r})$. At our EP3, the three eigenmodes coalesce and become self-orthogonal [16], leading to vanishing inner products $\left(\Psi_n^{\mathrm{L}}\right)^{\mathrm{T}} \Psi_n^{\mathrm{R}} = 0$, $n \in \{1, 2, 3\}$, as characterized by the so-called Petermann factor (PF),

$$\mathrm{PF}_n = \frac{||\Psi_n^{\mathrm{L}}||^2 ||\Psi_n^{\mathrm{R}}||^2}{|\left(\Psi_n^{\mathrm{L}}\right)^{\mathrm{T}} \Psi_m^{\mathrm{R}}|^2} \tag{10}$$

where $||...||^2$ is the usual L_2 norm given by $||\Psi||^2 = \Psi^{\mathrm{T}*}\Psi$. Figure 2(e,f) illustrates the divergence of the PF for all three modes as $\mathbf{k} \to \mathbf{k}^{\mathrm{EP3}}$. Note that there are also PF divergences associated with the M, D modes at the EP2 contours.

Local density of states.— The divergence of the Petermann Factor (PF) in open systems can lead to many important effects [11, 44]. In particular, the SE rate of emitters in resonant
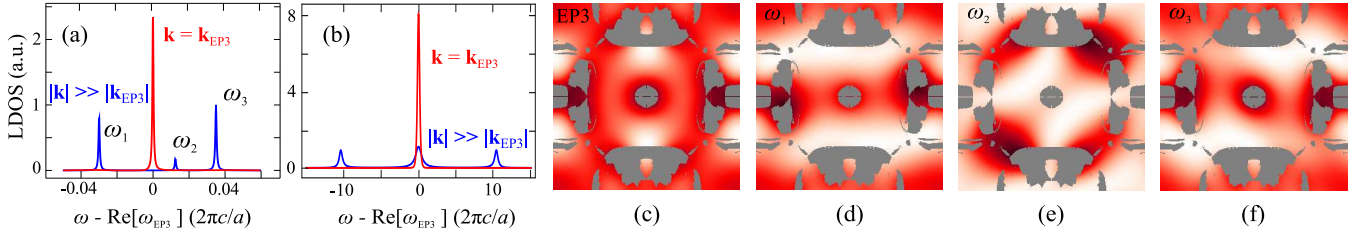
FIG. 3. (a) Local density of states (LDOS) at the center of the unit cell of the structure in Fig. 1, evaluated at either $\mathbf{k}^{EP3} \approx \{7, 1.8\} \times 10^{-5}(\frac{2\pi}{a})$ (red curves) or $\mathbf{k} = \{7, 1.8\} \times 10^{-2}(\frac{2\pi}{a}) \gg \mathbf{k}^{EP3}$ (blue curves). (b) Maximum (8-fold) LDOS enhancement associated with a EP3, computed via the reduced 3×3 Hamiltonian model of (3). (c)–(f) LDOS profiles evaluated at either ω_{EP3} or at the non-degenerate frequencies ω_1, ω_2, and ω_3, corresponding to the EP3 and far-away points described in (a). Note that the LDOS is evaluated only in air regions since the LDOS within a lossy medium formally diverges [43].

cavities is traditionally expressed via the PF (a generalization of the Purcell factor [44]), becoming most pronounced near EPs where the latter diverges [45]. More rigorously, however, the SE rate is given by the local density of states (LDOS), or electromagnetic Green's function (GF), which though enhanced turns out to be finite even at EPs [22]: coalescent eigenmodes no longer form a complete basis, requiring instead an augmented basis of associated Jordan modes and hence a different definition of LDOS. Such an expansion was recently employed in Ref. 22 to demonstrate limits to LDOS at EP2s in both passive and active media; here, we extend these results to the case of EP3s.

The LDOS at an EP3 can be obtained from the diagonal elements of the imaginary part of the dyadic GF [SM]:

$$\mathbb{G}_{EP3} \approx \frac{\Psi_{EP3}^R(\Phi_I^L)^T}{(\omega^2 - \omega_{EP3}^2)^3} + \frac{\Psi_{EP3}^R(\Phi_I^L)^T + \Phi_I^R(\Psi_{EP3}^L)^T}{(\omega^2 - \omega_{EP3}^2)^2} + \frac{\Psi_{EP3}^R(\Phi_{II}^L)^T + \Phi_I^R(\Phi_I^L)^T + \Phi_{II}^R(\Psi_{EP3}^L)^T}{\omega^2 - \omega_{EP3}^2}. \quad (11)$$

Equation 11 involves a complicated sum of cubic, quadratic, and linear Lorentzian profiles weighted by the outer products of the only surviving left (right) eigenmode $\Psi_{EP3}^{(L,R)}$ and the two associated Jordan vectors $\Phi_{(I,II)}^{(L,R)}$, determined by the third-order Jordan decomposition of the Maxwell eigenproblem,

$$A_{EP3}\Psi_{EP3}^R = \omega_{EP3}^2 \Psi_{EP3}^R \quad (12)$$
$$A_{EP3}\Phi_I^R = \omega_{EP3}^2 \Phi_I^R + \Psi_{EP3}^R \quad (13)$$
$$A_{EP3}\Phi_{II}^R = \omega_{EP3}^2 \Phi_{II}^R + \Phi_I^R, \quad (14)$$

and its associated dual. Equation 11 reveals that the LDOS spectrum $\sim -\mathrm{Im}[\mathrm{Tr}(\mathbb{G})]$ can vary dramatically depending on position, frequency, and decay rates.

Figure 3(a) shows the LDOS spectra at the center of the unit cell $\mathbf{r}_0$, evaluated at either $\mathbf{k}^{EP3}$ (red curves) or a point $\mathbf{k} = \{7, 1.8\} \times 10^{-2}(2\pi/a) \gg \mathbf{k}^{EP3}$ (blue curves) far away from the EP3, demonstrating an enhancement factor of ≈ 2.33 in this geometry. Even greater enhancements are possible under different loss profiles, i.e., γ_M, γ_D and γ_Q, as illustrated by the following analysis based on the reduced Hamiltonian framework above. In particular, the GF at a given location in

the unit cell can be directly related to the diagonal entries of the resolvent of $\mathcal{H}$, defined as $G \equiv (\mathcal{H} - \omega\mathbb{I})^{-1}$. For example, the third entry of G yields the LDOS at points where the intensity of the quadrupole mode dominates. Consider a scenario in which only the monopole mode has a finite lifetime, i.e., $\gamma_M = \gamma$ while $\gamma_D = \gamma_Q = 0$. It follows from (3) and (11) that the LDOS in this case is given by,

$$-\mathrm{Im}\{G_{EP3}[3,3]\} \approx -\frac{2\gamma^2}{27}\frac{\bar{\gamma}^3 - 3\bar{\gamma}(\mathrm{Re}[\omega_{EP3}] - \omega)^2}{(\mathrm{Re}[\omega_{EP3}] - \omega)^2 + \bar{\gamma}^2]^3}$$
$$+\frac{\gamma}{3}\frac{\bar{\gamma}^2 - (\mathrm{Re}[\omega_{EP3}] - \omega)^2}{[(\mathrm{Re}[\omega_{EP3}] - \omega)^2 + \bar{\gamma}^2]^2} - \frac{\bar{\gamma}}{(\mathrm{Re}[\omega_{EP3}] - \omega)^2 + \bar{\gamma}^2}, \quad (15)$$

where $\bar{\gamma} \equiv \gamma/3$. Moreover, the peak LDOS at $\omega = \mathrm{Re}[\omega_{EP3}]$ is found to be $8/\gamma$, corresponding to an 8-fold enhancement relative to the peak LDOS far away from the EP3. Such an enhancement is illustrated in Fig. 3(b), which also reveals the highly non-Lorentzian spectrum associated with this EP3.

It is possible to exploit a simple sum rule, namely that the spectrally integrated LDOS is a constant [46], to predict the maximum enhancement possible for an EP of arbitrary order n. In particular, the integrated LDOS of an order-n Lorentzian of the form $L_n(\omega) = \frac{\gamma^{2n-1}c_n}{[(\omega - \mathrm{Re}[\omega_{EPn}])^2 + \gamma^2]^n}$ is $S_n(\omega) = \int d\omega\, L_n(\omega) = \frac{c_n\sqrt{\pi}\Gamma[n-\frac{1}{2}]}{\Gamma[n]}$, where Γ is the gamma function. It follows from the sum rule that $nS_1(\omega) = S_n(\omega)$ and, consequently, that $c_n/c_1 = \frac{\sqrt{\pi}\Gamma[n+1]}{\Gamma[n-\frac{1}{2}]} \sim \sqrt{n^3}$ for large $n \gg 1$. In the case of an EP3, the maximum enhancement $c_3/c_1 = 8$, which is realized in the scenario discussed above.

Concluding remarks.— The inverse-design approach described above is a powerful, general-purpose tool for engineering complex and unusual photonic properties, such as spectral degeneracies, leading to unconventional structures that arguably could not have been conceived by intuition alone. Although fabrication of the resulting "bar-code" structures may prove challenging at visible wavelengths using currently available technologies, future experimental realizations are entirely feasible in the far-infrared to microwave regimes, where complex features can be straightforwardly fabricated in polymers and ceramics with the aid of computerized ma-

chining, 3D printing, laser cutting, additive manufacturing, or two-photon lithography [47–49]. Furthermore, while our predictions offer a proof of principle based on a particular PhC platform, the same inverse-design techniques can be applied to consider higher-order EPs as well as other topologies, including localized cavities. Our ongoing work in this regard includes application of TO to problems related to the design of chiral modes, photonic Weyl points, topological insulators, and omnidirectional Dirac-cone, zero-index meta-materials.

* zinlin@g.harvard.edu

[1] Song-Liang Chua, Ling Lu, Jorge Bravo-Abad, John D. Joannopoulos, and Marin Soljačić. Larger-area single-mode photonic crystal surface-emitting lasers enabled by an accidental dirac point. *Opt. Lett.*, 39(7):2072–2075, Apr 2014.

[2] Xiangdong Zhang. Observing *Zitterbewegung* for photons near the dirac point of a two-dimensional photonic crystal. *Phys. Rev. Lett.*, 100:113903, 2008.

[3] Xueqin Huang, Yun Lai, Zhi Hong Hang, Huihuo Zheng, and C. T. Chan. Dirac cones induced by accidental degeneracy in photonic crystals and zero-refractive-index materials. *Nat Mater*, 10(8):582–586, 08 2011.

[4] Yang Li, Shota Kita, Philip Muñoz, Orad Reshef, Daryl I. Vulis, Mei Yin, Marko Lončar, and Eric Mazur. On-chip zero-index metamaterials. *Nat Photon*, 9(11):738–742, 11 2015.

[5] S. Raghu and F. D. M. Haldane. Analogs of quantum-hall-effect edge states in photonic crystals. *Phys. Rev. A*, 78:033834, 2008.

[6] Alexander B. Khanikaev, S. Hossein Mousavi, Wang-Kong Tse, Mehdi Kargarian, Allan H. MacDonald, and Gennady Shvets. Photonic topological insulators. *Nat Mater*, 12(3):233–239, 2013.

[7] Ling Lu, Chen Fang, Liang Fu, Steven G. Johnson, John D. Joannopoulos, and Marin Soljacic. Symmetry-protected topological photonic crystal in three dimensions. *Nat Phys*, 12(4):337–340, 2016.

[8] Bo Zhen, Chia Wei Hsu, Yuichi Igarashi, Ling Lu, Ido Kaminer, Adi Pick, Song-Liang Chua, John D. Joannopoulos, and Marin Soljacic. Spawning rings of exceptional points out of dirac cones. *Nature*, 525(7569):354–358, 09 2015.

[9] Nimrod Moiseyev. *Non-Hermitian Quantum Mechanics*. Cambridge University Press, 2011.

[10] Tosio Kato. *Perturbation theory for linear operators*. Springer-Verlag Berlin Heidelberg, 1995.

[11] Michael V. Berry. Physics of nonhermitian degeneracies. *Czechoslovak Journal of Physics*, 54(10), 2004.

[12] W D Heiss. The physics of exceptional points. *Journal of Physics A: Mathematical and Theoretical*, 45(44):444016, 2012.

[13] Carl M. Bender and Stefan Boettcher. Real spectra in non-hermitian hamiltonians having $\mathcal{PT}$ symmetry. *Phys. Rev. Lett.*, 80:5243–5246, 1998.

[14] Christian E. Ruter, Konstantinos G. Makris, Ramy El-Ganainy, Demetrios N. Christodoulides, Mordechai Segev, and Detlef Kip. Observation of parity-time symmetry in optics. *Nat Phys*, 6(3):192–195, 2010.

[15] A. Guo, G. J. Salamo, D. Duchesne, R. Morandotti, M. Volatier-Ravat, V. Aimez, G. A. Siviloglou, and D. N. Christodoulides. Observation of $\mathcal{PT}$-symmetry breaking in complex optical potentials. *Phys. Rev. Lett.*, 103:093902, 2009.

[16] Mei C. Zheng, Demetrios N. Christodoulides, Ragnar Fleischmann, and Tsampikos Kottos. $\mathcal{PT}$ optical lattices and universality in beam dynamics. *Phys. Rev. A*, 82:010103, 2010.

[17] Hamidreza Ramezani, Tsampikos Kottos, Vassilios Kovanis, and Demetrios N. Christodoulides. Exceptional-point dynamics in photonic honeycomb lattices with $\mathcal{PT}$ symmetry. *Phys. Rev. A*, 85:013818, 2012.

[18] Stefano Longhi and Giuseppe Della Valle. Optical lattices with exceptional points in the continuum. *Phys. Rev. A*, 89:052132, 2014.

[19] Li Ge and A. Douglas Stone. Parity-time symmetry breaking beyond one dimension: The role of degeneracy. *Phys. Rev. X*, 4:031011, 2014.

[20] Alexander Cerjan, Aaswath Raman, and Shanhui Fan. Exceptional contours and band structure design in parity-time symmetric photonic crystals. *arXiv*, (arXiv:1601.05489), 2016.

[21] Michael V. Berry. Mode degeneracies and the petermann excess-noise factor for unstable lasers. *Journal of Modern Optics*, 50(1):63–81, 2003.

[22] A. Pick, B. Zhen, O. D. Miller, C. W. Hsu, F. Hernandez, A. W. Rodriguez, M. Soljačić, and S. G. Johnson. General theory of spontaneous emission near exceptional points. *arXiv*, 1604.06478, 2016.

[23] C. Dembowski, B. Dietz, H.-D. Gräf, H. L. Harney, A. Heine, W. D. Heiss, and A. Richter. Observation of a chiral state in a microwave cavity. *Phys. Rev. Lett.*, 90:034101, 2003.

[24] Zin Lin, Hamidreza Ramezani, Toni Eichelkraut, Tsampikos Kottos, Hui Cao, and Demetrios N. Christodoulides. Unidirectional invisibility induced by $\mathcal{PT}$-symmetric periodic structures. *Phys. Rev. Lett.*, 106:213901, 2011.

[25] Liang Feng, Ye-Long Xu, William S. Fegadolli, Ming-Hui Lu, JoséE. B. Oliveira, Vilson R. Almeida, Yan-Feng Chen, and Axel Scherer. Experimental demonstration of a unidirectional reflectionless parity-time metamaterial at optical frequencies. *Nat Mater*, 12(2):108–113, 2013.

[26] M. Liertzer, Li Ge, A. Cerjan, A. D. Stone, H. E. Türeci, and S. Rotter. Pump-induced exceptional points in lasers. *Phys. Rev. Lett.*, 108:173901, 2012.

[27] Hossein Hodaei, Mohammad-Ali Miri, Matthias Heinrich, Demetrios N. Christodoulides, and Mercedeh Khajavikhan. Parity-time–symmetric microring lasers. *Science*, 346(6212):975–978, 2014.

[28] Liang Feng, Zi Jing Wong, Ren-Min Ma, Yuan Wang, and Xiang Zhang. Single-mode laser by parity-time symmetry breaking. *Science*, 346(6212):972–975, 2014.

[29] T. Gao, E. Estrecho, K. Y. Bliokh, T. C. H. Liew, M. D. Fraser, S. Brodbeck, M. Kamp, C. Schneider, S. Hofling, Y. Yamamoto, F. Nori, Y. S. Kivshar, A. G. Truscott, R. G. Dall, and E. A. Ostrovskaya. Observation of non-hermitian degeneracies in a chaotic exciton-polariton billiard. *Nature*, 526(7574):554–558, 2015.

[30] E M Graefe, U Günther, H J Korsch, and A E Niederle. A non-hermitian $\mathcal{PT}$ symmetric bose–hubbard model: eigenvalue rings from unfolding higher-order exceptional points. *Journal*

of Physics A: Mathematical and Theoretical, 41(25):255206, 2008.

[31] Jung-Wan Ryu, Soo-Young Lee, and Sang Wook Kim. Analysis of multiple exceptional points related to three interacting eigenmodes in a non-hermitian hamiltonian. *Phys. Rev. A*, 85:042101, 2012.

[32] W D Heiss and G Wunner. Resonance scattering at third-order exceptional points. *Journal of Physics A: Mathematical and Theoretical*, 48(34):345203, 2015.

[33] Kun Ding, Guancong Ma, Meng Xiao, Z. Q. Zhang, and C. T. Chan. Emergence, coalescence, and topological properties of multiple exceptional points and their experimental realization. *Phys. Rev. X*, 6:021007, 2016.

[34] By accidental degeneracy, we mean that the frequency collision is neither induced nor protected by any underlying point symmetry, but rather is entirely fashioned out of the detailed morphology of the photonic unit cell, designed via brute-force topology optimization techniques.

[35] Jun Mei, Ying Wu, C. T. Chan, and Zhao-Qing Zhang. First-principles study of dirac and dirac-like cones in phononic and photonic crystals. *Phys. Rev. B*, 86:035141, 2012.

[36] Kazuaki Sakoda. Proof of the universality of mode symmetries in creating photonic dirac cones. *Opt. Express*, 20(22):25181–25194, 2012.

[37] J.S. Jensen and O. Sigmund. Topology optimization for nanophotonics. *Laser and Photonics Reviews*, 5(2):308–321, 2011.

[38] Alexander Y. Piggott, Jesse Lu, Konstantinos G. Lagoudakis, Jan Petykiewicz, Thomas M. Babinec, and Jelena Vuckovic. Inverse design and demonstration of a compact and broadband on-chip wavelength demultiplexer. *Nature Photonics*, 9:374–377, 2015.

[39] Bing Shen, Peng Wang, and Rajesh Menon. An integrated-nanophotonics polarization beamsplitter with 2.4 x 2.4 um2 footprint. *Nature Photonics*, 9:378–382, 2015.

[40] Xiangdong Liang and Steven G. Johnson. Formulation for scalable optimization of microcavities via the frequency-averaged local density of states. *Opt. Express*, 21(25):30812–30841, Dec 2013.

[41] Zin Lin, Xiangdong Liang, Marko Lončar, Steven G. Johnson, and Alejandro W. Rodriguez. Cavity-enhanced second-harmonic generation via nonlinear-overlap optimization. *Optica*, 3(3):233–238, Mar 2016.

[42] Krister Svanberg. A class of globally convergent optimization methods based on conservative convex separable approximations. *SIAM Journal on Optimization*, pages 555–573, 2002.

[43] S. Scheel, L. Knöll, and D.-G. Welsch. Spontaneous decay of an excited atom in an absorbing dielectric. *Phys. Rev. A*, 60:4094–4104, 1999.

[44] K. Petermann. Calculated spontaneous emission factor for double-heterostructure injection lasers with gain-induced waveguiding. *IEEE J. Quant. Elect.*, 15(7):566–570, 1979.

[45] M. V. Berry. Mode degeneracies and the petermann excess-noise factor for unstable lasers. *J. of mod. opt.*, 50(1):63–81, 2003.

[46] S. M. Barnett and R. Loudon. Sum rule for modified spontaneous emission rates. *Phys. Rev. Lett.*, 77(12):2444, 1996.

[47] R.A. Borisov, G.N. Dorojkina, N.I. Koroteev, V.M. Kozenkov, S.A. Magnitskii, D.V. Malakhov, A.V. Tarasishin, and A.M. Zheltikov. Fabrication of three-dimensional periodic microstructures by means of two-photon polymerization. *Applied Physics B*, 67(6):765–767, 1998.

[48] Anders Clausen, Fengwen Wang, Jakob S. Jensen, Ole Sigmund, and Jennifer A. Lewis. Topology optimized architectures with programmable poisson's ratio over large deforma-

tions. *Advanced Materials*, 27(37):5523–5527, 2015.

[49] Caroline Pouya, Johannes T. B. Overvelde, Mathias Kolle, Joanna Aizenberg, Katia Bertoldi, James C. Weaver, and Pete Vukusic. Characterization of a mechanically tunable gyroid photonic crystal inspired by the butterfly parides sesostris. *Advanced Optical Materials*, 4(1):99–105, 2016.

[50] A. Taflove, A. Oskooi, and S. G. Johnson. *Advances in FDTD Computational Electrodynamics: Photonics and Nanotechnology*. Artech House, 2013.

[51] G. B. Arfken and H. J. Weber. *Mathematical Methods for Physicists*. Elsevier Academic Press, 2006.

[52] A. Mailybaev and A. P. Seyranian. On singularities of a boundary of the stability domain. *SIAM Journal on Matrix Analysis and Applications*, 21(1):106–128, 1999.

[53] G. Demange and E-M Graefe. Signatures of three coalescing eigenfunctions. *Journal of Physics A: Mathematical and Theoretical*, 45(2):025303, 2011.

[54] A. P. Seyranian and A. A. Mailybaev. *Multiparameter Stability Theory With Mechanical Applications*. World Scientific Publishing, 2003.

SUPPLEMENTARY MATERIALS

TOPOLOGY OPTIMIZATION

A typical topology optimization problem in photonics goes as follows. The objective is to maximize or minimize a given objective function f subject to certain constraints g over a set of free variables or degrees of freedom (DOF):

$$\max/\min f(\bar{\epsilon}_\alpha) \tag{16}$$

$$g(\bar{\epsilon}_\alpha) \leq 0 \tag{17}$$

$$0 \leq \bar{\epsilon}_\alpha \leq 1 \tag{18}$$

where the DOF are the normalized dielectric constants $\bar{\epsilon}_\alpha \in [0, 1]$ assigned to each pixel or voxel (indexed α) in a specified volume. Note that, in general, the index α denote Cartesian components $\{\alpha_x, \alpha_y, \alpha_z\}$, such that in a finite-difference grid, $\bar{\epsilon}_\alpha = \bar{\epsilon}(\mathbf{r}_\alpha) = \bar{\epsilon}(\alpha_x \Delta x, \alpha_y \Delta y, \alpha_z \Delta z)$. Depending on the choice of background (bg) and structural materials, $\bar{\epsilon}_\alpha$ is mapped onto position-dependent dielectric constant via $\epsilon_\alpha = (\epsilon - \epsilon_{\text{bg}}) \bar{\epsilon}_\alpha + \epsilon_{\text{bg}}$. Since we are interested in fabricatable structures, we primarily focus on binary dielectrics by avoiding intermediate values of $\bar{\epsilon}$. The binarity of the system can be enforced by penalizing the objective function or utilizing a variety of filter and regularization methods [37]. Typically, starting from a random initial guess or completely uniform space, the technique discovers complex structures automatically with the aid of powerful algorithms such as the method of moving asymptotes (MMA) [42], which typically require gradient information of the objective and constraint functions, i.e., $\frac{\partial f}{\partial \bar{\epsilon}_\alpha}$, $\frac{\partial g}{\partial \bar{\epsilon}_\alpha}$. For an electromagnetic problem, f and g are typically functions of the electric $\mathbf{E}$ or magnetic $\mathbf{H}$ fields integrated over some region, which are in turn solutions of Maxwell's equations under some incident current or field. In what follows, we exploit direct solution of the local
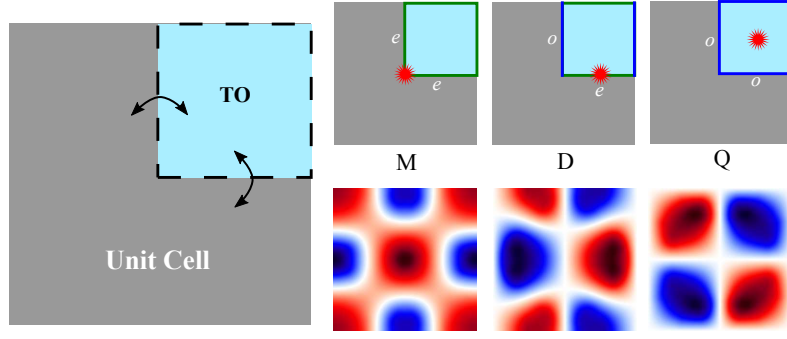
FIG. 4. Left: Schematic showing the design region (top-right quadrant) for topology optimization (TO) of a photonic crystal (PhC) unit cell at the Γ point. The design region is extended by mirror reflections to the remaining quadrants of the unit cell. Right: The position of a point source (bright red dot) as well as choice of even (e) or odd (o) boundary conditions which determine the nodal structure of the resulting modes.

Maxwell's equations (a partial differential equation),

$$\nabla \times \frac{1}{\mu} \nabla \times \mathbf{E} - \epsilon(\mathbf{r})\omega^2 \mathbf{E} = i\omega \mathbf{J}, \qquad (19)$$

to obtain the steady-state $\mathbf{E}(\mathbf{r}; \omega)$ in response to incident currents $\mathbf{J}(\mathbf{r}, \omega)$ at frequency ω. While solution of (19) is straightforward and commonplace, the key to making optimization problems tractable is to obtain a fast-converging and computationally efficient adjoint formulation of the problem [37]. Within the scope of TO, this requires efficient calculations of the gradients $\frac{\partial f}{\partial \bar{\epsilon}_\alpha}$, $\frac{\partial g}{\partial \bar{\epsilon}_\alpha}$ at every pixel α, which we perform by exploiting the powerful adjoint-variable method (AVM), described in [37]. Essentially, instead of having to calculate the $\frac{\partial f}{\partial \bar{\epsilon}(\mathbf{r})}$ for every spatial point $\mathbf{r}$, AVM offers the gradient over the entire optimization region at the cost of a *single* (additional) solution of Maxwell's equation, and is therefore key to the tractability of the optimization process.

LDOS FORMULATION

Recent work [40] considered topology optimization of the cavity Purcell factor by exploiting the concept of local density of states (LDOS). In particular, the equivalence between the LDOS and power radiated by a *point* dipole can be exploited to reduce Purcell-factor maximization problems to a series of small scattering calculations. The objective function is chosen as $\max_{\bar{\epsilon}} f(\bar{\epsilon}(\mathbf{r}); \omega) = -\text{Re}\left[\int d\mathbf{r} \, \mathbf{J}^* \cdot \mathbf{E}\right]$, where $\mathbf{J} = \delta(\mathbf{r} - \mathbf{r}_0)\hat{\mathbf{e}}_j$. The gradient field $\frac{\partial f}{\partial \bar{\epsilon}}$ is given by [40]

$$\frac{\partial f}{\partial \bar{\epsilon}(\mathbf{r})} = \text{Re}\left[i\omega(\epsilon - \epsilon_{\text{bg}})\mathbf{E} \cdot \mathbf{E}\right] \qquad (20)$$

A key realization in [40] is that instead of maximizing the LDOS at a single discrete frequency ω, a better-posed problem is that of maximizing the frequency-averaged f in the vicinity of ω, denoted by $\langle f \rangle = \int d\omega' \, \mathcal{W}(\omega'; \omega, \Gamma) f(\omega')$, where $\mathcal{W}$ is some weight function defined over a specified bandwidth Γ. Using contour integration techniques, the frequency integral can be conveniently replaced by a single evaluation of f at a

complex frequency $\omega + i\Gamma$ [40]. For a fixed Γ, the frequency average effectively forces the algorithm to favor minimizing V over maximizing Q; the latter can be enhanced over the course of the optimization by gradually winding down Γ [40]. A major merit of this formulation is that it features a mathematically well-posed objective as opposed to a direct maximization of the cavity Purcell factor $\frac{Q}{V}$, allowing rapid convergence into extremal solutions. Here, we note that the LDOS formulation offers a natural elegant tool for the inverse design of any kind of resonant mode, not just the localized cavity modes considered in [40]. In particular, it can be successfully applied for the inverse design of extended Bloch modes in a periodic medium for an arbitrary choice of Bloch wave vector $\mathbf{k}$. Although this work has focused on Bloch modes at the Γ point, we have found that the algorithm can be employed with similar ease to design photonic spectra at $\mathbf{k} \neq 0$.

A simple extension of the optimization formula from a single-mode problem to the inverse design of a multi-mode degeneracy is to maximize the minimum of a collection of LDOSs corresponding to different $\mathbf{J}$'s at the exact same frequency ω. Here, the objective assumes the form of a so-called *maximin* problem: $\max_{\bar{\epsilon}(\mathbf{r})} \min_n \left\{ f(\omega; \mathbf{J}_n) \right\}$, which requires solving *separate* scattering problems for the distinct sources $\mathbf{J}_n$ at the same frequency ω. In practice, we replace the maximin objective with an equivalent formulation [37]: $\max t$, subject to $t - f_n \leq 0$.

DESIGN OF AN ACCIDENTAL THIRD-ORDER DIRAC DEGENERACY AT THE Γ POINT

To design a third order Dirac degeneracy (D3), we maximize the minimum of $\left\{ f_{\text{M}}, \, f_{\text{D}}, \, f_{\text{Q}} \right\}$ at the Γ point, where M, D and Q denote monopolar, dipolar and quadrupolar transverse magnetic (TM) modes ($\hat{z} \times \mathbf{E} = 0$). For easier computations, we impose C_{2v} symmetry with mirror planes at the center of the unit cell. Note that the mirror planes are also essential for classifying modes by their even or odd transformation properties. In group theoretic language, the eigenmodes of

the PhC at Γ point transform according to distinct irreducible representations; specifically, M, D and Q modes belong to three *distinct* irreducible representations A_1, A_2 and B_1 of the group C_{2v}. In effect, the degrees of freedom (DOF) are restricted to one quadrant of the unit cell whereas the unique nodal structures of M, D and Q are enforced by a careful choice of boundary conditions as well as a judicious positioning of the point sources $\mathbf{J}$, as shown in Fig. 4. Under these settings, the optimization converges approximately within 500 iterations, taking less than two hours. During optimization, we also impose filter and penalization constraints [37] in order to avoid intermediate ϵ values.

Figure 5 shows two binary structures obtained by application of the aforementioned optimization technique and exhibiting the desired three-mode degeneracy to within 0.01% of the designated frequencies, $\omega_0 = 2\pi c/a$, where a is the lattice constant. While the details of the low-index structure [Fig. 5(a)] are described in the main text, here we focus on the high-index design [Fig. 5(b)], whose refractive index $n = 3.07$ and period $a = 0.6\,\lambda$. Noticeably, the high-index design possesses highly connected features (few isolated components) and should, therefore, be more readily fabricatable by conventional methods. For instance, the dielectric constant of alumina ceramics is ≈ 9.4 at 10 GHz, paving the way for fabrication and characterization of such a structure based on standard high-precision computerized machining of suitable alumina samples at microwave frequencies. The band structure of the high-index design exhibits a D3 of M, D and Q modes Fig. 5(b). Assuming loss $\text{Im}[\epsilon] = 0.02$ uniformly distributed throughout the dielectric material, leading to decay rates $\{\gamma_{\mathrm{M}}, \gamma_{\mathrm{D}}, \gamma_{\mathrm{Q}}\}/\omega_0 \approx \{9.83, 9.73, 9.78\} \times 10^{-4}$, we find that the EP3 occurs at $\mathbf{k}_{\mathrm{EP3}} = \{4.5, 2.9\} \times 10^{-6}(2\pi/a)$ and results in a Petermann factor $\approx 10^8$.

DESIGN OF A THIRD-ORDER EXCEPTIONAL POINT

In order to better understand the dispersion properties of the TO-designed PhC as well as to determine the existence of an EP3, we can approximate the band structure near the Γ point in terms of the degenerate modes at Γ, leading to an eigenproblem $\mathcal{H}\psi = \omega^2\psi$ based on the 3×3 Hamiltonian [35]:

$$\mathcal{H} = \begin{pmatrix} \omega_0^2 & p_{\mathrm{MD}}k_x & 0 \\ p_{\mathrm{MD}}^*k_x & \omega_0^2 & p_{\mathrm{QD}}k_y \\ 0 & p_{\mathrm{QD}}^*k_y & \omega_0^2 \end{pmatrix} \quad (21)$$

Note that under the approximation $\omega_0^2 - \omega^2 \approx 2\omega_0(\omega_0 - \omega)$ and substitution $p_{ij} = 2\omega_0 v_{ij}$, one is led to the simplified Hamiltonian (considered in the main text):

$$\mathcal{H} = \begin{pmatrix} \omega_0 & v_{\mathrm{MD}}k_x & 0 \\ v_{\mathrm{MD}}^*k_x & \omega_0 & v_{\mathrm{QD}}k_y \\ 0 & v_{\mathrm{QD}}^*k_y & \omega_0 \end{pmatrix} \quad (22)$$

Although (22) is easier to work with for deriving closed-form analytical expressions, to achieve better accuracy our predictions in the main text and discussion below are based on (21).

The introduction of a small $\text{Im}[\epsilon]$ yields the following non-Hermitian Hamiltonian:

$$\mathcal{H}' = \begin{pmatrix} (\omega_0 + i\gamma_{\mathrm{M}})^2 & p'_{\mathrm{MD}}k_x & 0 \\ -p'_{\mathrm{MD}}k_x & (\omega_0 + i\gamma_{\mathrm{D}})^2 & p'_{\mathrm{QD}}k_y \\ 0 & -p'_{\mathrm{QD}}k_y & (\omega_0 + i\gamma_{\mathrm{Q}})^2 \end{pmatrix} \quad (23)$$

Note that for sufficiently small $\text{Im}[\epsilon]$, $p'_{ij} \approx p_{ij}$ and $-p'_{ij} \approx p_{ij}^*$ and that the form of (23) maintains reciprocity since $\mathcal{H}^{\mathrm{T}}(\mathbf{k}) = \mathcal{H}(-\mathbf{k})$. For simplicity of notation, we will drop the prime with the understanding that any reference to $\mathcal{H}$ from here on refers to (23). The mode-mixing parameters p_{ij} can be computed from overlap integrals between the degenerate modes at the Γ point [35]. In particular, in the case of the low-index design ($n = 2$, see main text) where we have chosen $\text{Im}[\epsilon] = 0.005$, we obtain $\gamma/\omega_0 \sim 10^{-3}$, $p_{\mathrm{MD}} \approx 5.9i/(2\pi)$ and $p_{\mathrm{QD}} \approx 5.5i/(2\pi)$. With these parameters in hand, we can determine the location of the EP3 by numerically solving (4)–(6) in the main text, resulting in the aforementioned values of $k_x^{\mathrm{EP3}} \approx 7 \times 10^{-5}\left(\frac{2\pi}{\lambda}\right)$ and $k_y^{\mathrm{EP3}} \approx 1.8 \times 10^{-5}\left(\frac{2\pi}{\lambda}\right)$.

While the topology-optimized binary design exhibits a trimodal degeneracy to an accuracy of $\lesssim 0.01\%$, we find that in order to access the EP3, further fine-tuning is necessary as is generally the case for parameter-sensitive exceptional points [8, 22]. In particular, for a fixed $\omega_{\mathrm{Q}} = \omega_0$, small deviations from some critical frequencies $\omega_{\mathrm{M}}^{\mathrm{c}}$ and $\omega_{\mathrm{D}}^{\mathrm{c}}$ introduces a small imaginary part to $\mathbf{k}_{\mathrm{EP3}}$. Figure 6 quantifies the magnitude of $\text{Im}[\mathbf{k}_{\mathrm{EP3}}]$ as a function of two bandgap parameters $\delta\omega_{\mathrm{M}}$ and $\delta\omega_{\mathrm{D}}$, defined such that $\omega_{\mathrm{M}} = \omega_0 + \delta\omega_{\mathrm{M}}$ and $\omega_{\mathrm{D}} = \omega_0 + \delta\omega_{\mathrm{D}}$. As observed, the imaginary part of $\mathbf{k}_{\mathrm{EP3}}$ vanishes when $\delta\omega_{\mathrm{M}} = \delta\omega_{\mathrm{M}}^{\mathrm{c}} \sim -10^{-7}$ and $\delta\omega_{\mathrm{D}} = \delta\omega_{\mathrm{D}}^{\mathrm{c}} \sim -10^{-9}$, signaling the appearance of a EP3 on the real $\mathbf{k}$ plane. While there are many post-fabrication fine-tuning techniques (such as oxidation, thermal, free-carrier, or laser tuning), in our numerical experiment, we simply fine-tune a few strategic pixels in the PhC design to vary ω_{M} and ω_{D} while keeping ω_{Q} fixed, repeatedly solving the full Maxwell eigenproblems until the Petermann Factor $\sim 10^9$.

GREEN'S FUNCTION AT A THIRD-ORDER EP

Non-orthogonality of the modes in open resonators can lead to significantly enhanced spontaneous emission rates [44]. This effect becomes most pronounced near exceptional points [45], where the modes become self-orthogonal. The figure of merit for computing spontaneous emission rates is the local density of states (LDOS), which is proportional to the imaginary part of the Green's function (GF) [50]. Near non-degenerate resonances, the GF can be expressed using the standard modal expansion formula [51]:

$$G = \sum_i \frac{1}{\omega^2 - \omega_i^2} \cdot \frac{\Psi_i^{\mathrm{R}}(\Psi_i^{\mathrm{L}})^T}{(\Psi_i^{\mathrm{L}})^T \Psi_i^{\mathrm{R}}}. \quad (24)$$

The right eigenvectors Ψ_i^{R} and eigenvalues ω_i are outgoing solutions of Maxwell's equations or, more explicitly, satisfy the
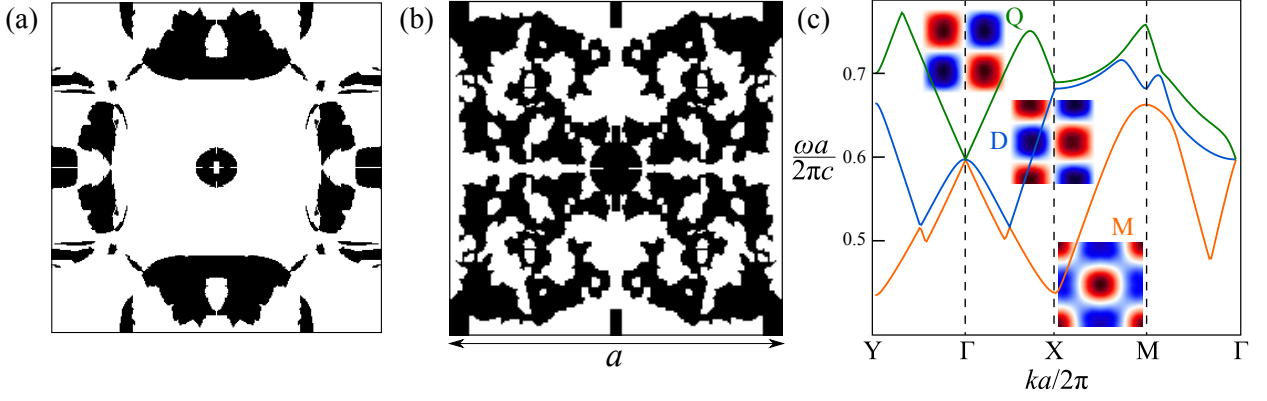
FIG. 5. Detailed images of inverse-designed PhC unit cells comprising either (a) low-index ($n = 2$) or (b) high-index ($n = 3.07$) dielectric materials in air, and supporting third-order Dirac degeneracies. Black/white represent dielectric/air regions. The lattice constants of the cells are $a = 1.05\,\lambda$ and $a = 0.6\,\lambda$, respectively, where λ denotes the design wavelength. Each pixel has dimensions $\approx 0.003 \times 0.003a^2$. (c) Band structure of the high-index structure, demonstrating the conical, Dirac dispersion around a tri-modal Dirac degeneracy, involving monopolar (M), dipolar (D), and quadrupolar (Q) modes, at the Γ point.
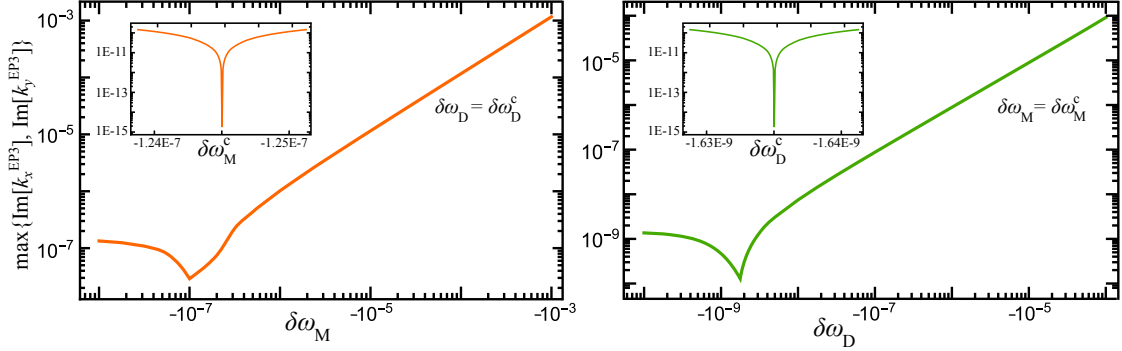

FIG. 6. Left: Imaginary part of $\mathbf{k}^{\text{EP3}}$ as a function of gap parameter $\delta\omega_{\text{M}}$, with $\delta\omega_{\text{D}}$ fixed at the critical value $\delta\omega_{\text{D}}^{\text{c}}$. Note the approximately linear scaling of $\text{Im}[\mathbf{k}^{\text{EP3}}] \sim \delta\omega_{\text{M}}$ away from the critical point. The inset magnifies the vicinity of $\delta\omega_{\text{M}}^{\text{c}}$, the critical gap value at which $\text{Im}[\mathbf{k}^{\text{EP3}}]$ vanishes. Right: Same as left but exploring variations of $\delta\omega_{\text{D}}$ when $\delta\omega_{\text{M}}$ is fixed at $\delta\omega_{\text{M}}^{\text{c}}$.

eigenvalue problem: $A\Psi_i^{\text{R}} = \omega_i^2 \Psi_i^{\text{R}}$. Here, A is Maxwell's operator $\varepsilon^{-1}\nabla \times \nabla \times$ and ε is the dielectric permittivity. Left eigemodes are eigenvectors of the transposed operator $A^T \Psi_i^{\text{L}} = \omega_i^2 \Psi_i^{\text{L}}$, where $A^T \equiv \nabla \times \nabla \times \varepsilon^{-1}$. The derivation of (24) relies on the assumption that the set of eigenvectors of A spans the Hilbert space, which breaks down at EPs due to the coalescence of both the eigenvalues and eigenvectors. In what follows, we derive an eigenvalue expansion formula for the GF that is valid at third-order exceptional points (EP3). Our derivation follows three main steps (as in [22]): First, we use perturbation theory to express the eigenvalues ω_i and eigenmodes Ψ_i^{L} near the EP in terms of the degenerate eigenvalue and Jordan-chain vectors and an associated perturbative parameter. We then substitute these expressions into (24). Lastly, we take the limit as one approaches the EP.

Let the Maxwell operator $A(p)$ be a parameter-dependent operator supporting a EP3 at $p = 0$. The Jordan chain vectors

of $A_{\text{EP3}} \equiv A(0)$ satisfy the relations [52, 53]:

$$A_{\text{EP3}}\Psi_{\text{EP3}}^{\text{R}} = \omega_{\text{EP3}}^2 \Psi_{\text{EP3}}^{\text{R}} \tag{25}$$

$$A_{\text{EP3}}\Phi_{\text{I}}^{\text{R}} = \omega_{\text{EP3}}^2 \Phi_{\text{I}}^{\text{R}} + \Psi_{\text{EP3}}^{\text{R}} \tag{26}$$

$$A_{\text{EP3}}\Phi_{\text{II}}^{\text{R}} = \omega_{\text{EP3}}^2 \Phi_{\text{II}}^{\text{R}} + \Phi_{\text{I}}^{\text{R}}, \tag{27}$$

with the duals obtained by letting $A \to A^T$ and $R \to L$, leading to the following orthogonality relations:

$$(\Psi_{\text{EP3}}^{\text{L}})^T \Psi_{\text{EP3}}^{\text{R}} = 0$$
$$(\Phi_{\text{I}}^{\text{L}})^T \Psi_{\text{EP3}}^{\text{R}} = (\Psi_{\text{EP3}}^{\text{L}})^T \Phi_{\text{I}}^{\text{R}} = 0$$
$$(\Psi_{\text{EP3}}^{\text{L}})^T \Phi_{\text{II}}^{\text{R}} = (\Phi_{\text{II}}^{\text{L}})^T \Psi_{\text{EP3}}^{\text{R}} = (\Phi_{\text{I}}^{\text{L}})^T \Phi_{\text{I}}^{\text{R}} \tag{28}$$

In order to uniquely define the above chain vectors, we choose the additional normalization conditions:

$$(\Psi_{\text{EP3}}^{\text{L}})^T \Phi_{\text{II}}^{\text{R}} = (\Phi_{\text{II}}^{\text{L}})^T \Psi_{\text{EP3}}^{\text{R}} = (\Phi_{\text{I}}^{\text{L}})^T \Phi_{\text{I}}^{\text{R}} = 1$$
$$(\Phi_{\text{II}}^{\text{L}})^T \Phi_{\text{I}}^{\text{R}} = (\Phi_{\text{I}}^{\text{L}})^T \Phi_{\text{II}}^{\text{R}}0 = 0$$
$$(\Phi_{\text{II}}^{\text{L}})^T \Phi_{\text{II}}^{\text{R}} = 0. \tag{29}$$

When the LDOS is dominated by three non-degenerate resonances, one can approximate the full GF via (24) by keeping only three terms in the sum. (This requires that the three resonances ω_i be spectrally separated from the rest of the eigenvalues and that G be evaluated at $\omega \approx \mathrm{Re}[\omega_i]$). Near the EP, $A(p)$ can can be written as [22]:

$$A(p) = A_{\mathrm{EP3}} + pA_1 + p^2 A_2 + \ldots, \qquad (30)$$

from which it follows that the eigenvalues and eigenvectors of $A(p)$ can be expanded in Puiseux series [54],

$$\omega_i^2 = \omega_{\mathrm{EP3}}^2 + p^{\frac{1}{3}}\omega_1^2 + p^{\frac{2}{3}}\omega_2^2 + p\,\omega_3^2 + p^{\frac{4}{3}}\omega_4^2 \ldots \qquad (31)$$

$$\Psi_i = \Psi_{\mathrm{EP3}}^{R} + p^{\frac{1}{3}}\Psi_1 + p^{\frac{2}{3}}\Psi_2 + p\,\Psi_3 + p^{\frac{4}{3}}\Psi_4 \ldots \qquad (32)$$

reducing to the eigenvalues and eigenvectors of A_{EP3} in the limit $p \to 0$. (Note that one can write similar expressions for the left eigenvectors.) Using Eqs. (30-32) and taking the limit as $p \to 0$, we arrive at (11) in the main text, describing the GF at a EP3. Note that in order to obtain the correct limit, one needs to keep terms up to $\mathcal{O}(p^{\frac{5}{3}})$ in Eqs. (30-32).